Chemistry Central Journal

RESEARCH ARTICLE

Open Access

CrossMark

Synthesis of multifunctional activated carbon nanocomposite comprising biocompatible flake nano hydroxyapatite and natural turmeric extract for the removal of bacteria and lead ions from aqueous solution

H. D. A. Chathumal Jayaweera[1], Induni Siriwardane[1,2], K. M. Nalin de Silva[1,2] and Rohini M. de Silva[1*]

Abstract

Clean water, which is free from pathogens and toxic chemicals, is vital to human health. The blue planet is encountering remarkable challenges in meeting the ever-increasing demands of clean water. The intention of this research study was to develop a water filter material that is capable of removing bacterial contaminants and heavy metals from fresh water using cost effective and easily fabricated biocompatible filter material. For this purpose, granular activated carbon (GAC) was coated with both hydroxyapatite (HAP) nanoflakes and turmeric extract (TE) (HAP/TE/GAC) which had been extracted from natural turmeric powder. In addition, GAC was coated only with HAP nanoflakes to synthesize HAP coated GAC (HAP/GAC) composite. Prepared HAP/GAC and HAP/TE/GAC were characterized using Fourier-transform infrared spectroscopy, X-ray diffractometry, scanning electron microscopy and UV–visible spectrophotometry. Antibacterial effect of the prepared nanocomposites, HAP/GAC and HAP/TE/GAC was compared with neat GAC using Gram-negative bacteria *Escherichia coli*. Results showed that antibacterial studies of the synthesized nanocomposites exhibit effective antibacterial activity against *E. coli* compared with neat GAC alone. However, the composite HAP/TE/GAC revealed better activity than HAP/GAC. Heavy metal adsorption ability of the synthesized composites was carried out using Pb^{2+} ions at room temperature at different time intervals and different pH levels. The equilibrium adsorption data were assessed via Langmuir and Freundlich adsorption isotherm models for neat GAC, HAP/GAC and HAP/TE/GAC at pH 6. The equilibrium adsorption data for GAC, HAP/GAC and HAP/TE/GAC were well fitted with both Freundlich and Langmuir isotherm models in the given Pb^{2+} concentrations. The HAP/TE/GAC composite is capable of maintaining the natural function of GAC in addition to removal of bacterial contaminants and heavy metals, which can be used as a point-of-use water filter material.

Keywords: Hydroxyapatite, Turmeric extract, Activated carbon, Nano composites, Adsorption

Introduction

Water is one of the vital enablers of life on earth. Water envisioned for human consumption is universally accepted to be free from chemical constituents and micro-organisms in amounts which would provide a

hazard to health. For a healthy person around 4–6 L of drinking water is the recommended amount and therefore it is extremely important to get access to clean water free from both chemical and biological contaminants. Consequently, purification of water for drinking purpose has become an important area of attention in the world [1]. Through purification removal of turbidity, organic contaminants, microorganisms and heavy metals from potable water sources are expected. In the recent past, there is an increased use of metallic substances in

*Correspondence: rohini@chem.cmb.ac.lk
[1] Department of Chemistry, University of Colombo, Colombo 00300, Sri Lanka
Full list of author information is available at the end of the article

Jayaweera *et al. Chemistry Central Journal* (2018) 12:18

Page 2 of 14

industries and this has resulted an accumulation of heavy metals in aquatic environment contaminating both surface and underground water sources [2]. It has been frequently observed that the amount of heavy metals such as lead (Pb), arsenic (As), cadmium (Cd), mercury (Hg), zinc (Zn), chromium (Cr), copper (Cu), silver (Ag) and iron (Fe) get accumulated due to most of the industrial actions [3, 4]. These heavy metals are known as 'silent killers' as this leads to many health problems including hyperpigmentation, hypopigmentation, kidney and gastrointestinal tract related disorders [3]. In addition, heavy metals are known to cause cancerous effect and has been observed in many occasions [5]. Of these heavy metals, Pb is one of the most abundant pollutant and this has been the subject of many research. Lead is known to cause many diseases leading to impaired fertility, mortality due to cardiovascular diseases and variety of neurodevelopmental outcomes [3, 6]. According to the World Health Organization (WHO) the provisional guideline value for lead is 0.01 mg/L [3]. On the other hand, it is widely observed that the presence of biological contaminants such as viruses, bacteria and protozoans in contaminated water lead to severe health effects in human. Often found types of viruses include Hepatitis A & E [3], Enterovirus [3] and Adenovirus [3, 7]. As it for bacteria *Escherichia coli* [3, 7], *Vibrio cholera* [3], *Salmonella* species [7] and *Shigella* [3, 7] are among the most common types available in contaminated water. In addition, protozoans like *Cryptosporidium* species [7] and *Giardia* species [7] can also be found in drinking water. Generally, *E. coli* is being considered as the indicator bacteria for the water quality [3]. Several chemical and physical agents are being used to remove microorganisms from drinking water. Most of the disinfectants are strong oxidants and therefore during their course of oxidation there is a tendency to occur harmful byproducts [7] which could damage healthy cells. As a result, the use of these disinfectants are limited and the attention is shifted to those that are not strong oxidants. As far as removal of heavy metals are concerned, several techniques such as precipitation [8, 9], reduction, ion-exchange [10, 11], adsorption [12, 13], electrochemical processes [14, 15] and reverse osmosis [16, 17] have been used. In recent past, the consideration has shifted towards nanomaterials in water purification due to their super sorption ability. On this regard, many nanomaterials, namely, iron oxide [18, 19], ZnO [20, 21], hydroxyapatite (HAP) [22], carbon nanotubes (CNT) [23–25] are used to remove heavy metals. Of which HAP records a greater potential in removing several heavy metals from contaminated water as well as exhibits a considerable amount of antibacterial property [22, 26]. In addition, many other engineered nanomaterials such as, Ag [27], TiO_2 [28] and C_{60} [29, 30] derivatives have demonstrated strong antimicrobial properties. The application of these materials are limited mainly due to toxicity caused due to the production of reactive oxygen species and various other effects [29].

Even though, there are many methods available to eliminate heavy metals and biological contaminants separately, the methods available to eliminate both of these contaminants simultaneously are scarce [26, 31].

Activated carbon has attracted as one of the best adsorbent materials due to its capacity to remove unpleasant tastes, odors, color and various chemicals from water [32]. The mechanism of adsorption in activated carbon differs for organic and inorganic contaminants [33]. Although activated carbon efficiently removes majority of organic contaminants, it is less effective in removing many heavy metals and micro-organisms in water [34]. In our previous study, the possibility of in situ coating of HAP nanorods on activated carbon and Pb^{2+} adsorption property was demonstrated [22]. Studies on bi-coated HAP and curcumin disclosed the removal of both heavy metals and microorganisms such as *E. coli* and *Staphylococcus aureus* from contaminated water [26, 31]. Turmeric powder, from the rhizome of the plant *Curcuma longa*, is a well-known ingredient in many oriental cuisines and contains hundreds of molecular constituents with diverse biological activities. Out of which, twelve molecules show anti-inflammatory whereas twenty molecules reveal antibiotic activity, while ten molecules are known to be anti-oxidants. In addition, there are 14 molecules displaying cancer preventive properties [35, 36]. The components of turmeric are called curcuminoids and usually 3–5% of curcuminoids are there in its raw state [35, 37]. Dicinnamoylmethane derivatives are the three main golden color components present in different proportions in curcuminoids. These includes curcumin, demethoxycurcumin and bisdemethoxycurcumin [37]. Generally, curcuminoids are water insoluble in acidic and neutral pH whereas soluble in alkali solutions. However, soluble in oils such as castor oil, peanut oil and ethyl oleate [38]. Out of the three main components, antibacterial effect of curcumin is known to exert via inhibiting the bacterial endotoxin induced cytokines secretion and related activation mechanisms, this leads to direct suppressing of bacterial cell growth [39]. The objective of our work is to develop a low cost biocompatible filter material consisting of both metal adsorption and antibacterial properties. In order to accomplish this HAP coated granular activated carbon (HAP/GAC) is further treated with turmeric extract. This turmeric covered HAP coated granular activated carbon (HAP/TE/GAC) was tested on both Pb^{2+} and *E. coli* bacteria.

Jayaweera *et al. Chemistry Central Journal* (2018) 12:18

Page 3 of 14

Materials and methods

Calcium nitrate tetrahydrate—$Ca(NO_3)_2 \cdot 4H_2O$ [Techno Pharmchem, Bahadurgarh, Haryana, India (30607)] was used as the calcium source, di-sodium hydrogen orthophosphate anhydrous LR—Na_2HPO_4 [S. D. Fine-Chem LTD (40158)] was used as the phosphate source with NH_3 solution—(MW = 17.03 g/mol, density = 0.91 g cm^{-3}, purity = 25% W/W, Merck Limited, Mumbai). Turmeric powder and GAC (Jacobi aquasorb AC) was used for the synthesis of the filter material. Distilled acetone was used as the solvent to prepare the extract from turmeric powder. When the solvent was not specified, double distilled water was used as the solvent. In order to prepare the Pb^{2+} solution, $Pb(NO_3)_2$ from Sigma-Aldrich was used and for the adjustment of pH hydrochloric acid from Daejung was used.

The solid reactants and the prepared nanocomposites were weighed using the analytical balance (CAS Cay 120). Drying was done using the electrical oven (Heraeus ST 6120). For the sonication purposes, sonicator (Sonorex super RK 1028 CH, BANDELIN Electronics, Berlin) was used. Fourier-transform infrared (FT-IR) spectra were obtained from Varian 660-IR, USA and KBr pellet technique was used to obtain the FT-IR spectra over the range of 400–4000 cm^{-1}. The preparation of the pellet was done by mixing 2 mg of the sample with 200 mg of oven dried spectroscopy grade KBr (Sigma-Aldrich). The UV–visible spectra were obtained from GENESYS 10S UV–Vis and the samples for the UV–visible spectroscopy were prepared by dissolving small portion of the precipitate in distilled ethanol. The surface morphology and the microstructural characteristics of the synthesized nanocomposites were analyzed using scanning electron microscope (HITACHI SU6600). X-ray diffraction analysis of the synthesized HAP/GAC and HAP/TE/GAC nanocomposites were performed on a Bruker D8 Focus X-ray powder Diffractometer using CuKα radiation (λ = 0.154 nm) over a 2Θ range of 3°–70°, with a step size of 0.020° and a step time of 1 s. The atomic absorption spectroscopy experiments were carried out using the instrument GBC 932 Plus flame atomic spectrometer.

The microbiology experiments were performed inside the Laminar Hood (Yamato, model ADS 160). The media for the bacterial growth were autoclaved using an Autoclave machine (KT-30SD, ALP Co. Ltd.) prior to the use. Glassware including petri plates were incubated at 180 °C for 2 h in an oven (Memmert Beschickung loading model 100–800) before use. Bacteria inoculated plates were incubated at 37 °C in an incubator (Memmert-Beschickung, model 100–800) for 18 h for growth.

Synthesis of HAP coated granular activated carbon

The coating of HAP on granular activated carbon was carried out using an in situ method. GAC (12.0 g) was added into a 20 mmol of $Ca(NO_3)_2 \cdot 4H_2O$ (0.4 M) solution. The temperature of the mixture was maintained at 80 °C. The mixture was stirred and a solution of 12 mmol Na_2HPO_4 (0.16 M) was added in a drop wise manner into the mixture. The pH of the mixture was maintained at 10 with the drop wise addition of conc. NH_3. Mixture was then vigorously stirred at its boiling point for about 3 h. The reaction mixture was then aged for about 24 h in room temperature. The product obtained was suction filtered and washed thoroughly with double distilled water until the pH of the filtrate become neutral. The washings were tested for Ca^{2+} ions in HAP using atomic absorption spectroscopy. The prepared HAP coated granular activated carbon was kept in the oven at 80 °C for about 3 h. The synthesized nanocomposite was characterized using FT-IR spectroscopy, scanning electron microscopy and X-ray diffractometry (XRD) analysis.

Preparation of turmeric extract from turmeric powder

Acetone was used as the solvent for the preparation of turmeric extract from turmeric powder. Distilled acetone (100 mL) was added into a portion of turmeric powder (60.0 g) and the mixture was sonicated at 50 °C for about 30 min. Then the mixture was suction filtered and the filtrate was collected. The product obtained after evaporating the solvent was an orange brown color residue. The turmeric extract was then characterized using FT-IR spectroscopy and UV–visible spectroscopy.

Synthesis of turmeric extract coated, HAP impregnated granular activated carbon

The nanocomposite synthesized was further coated with the turmeric extract. For this turmeric extract (3.0 g) was dissolved in acetone (50 mL) and added in a drop wise manner to the mixture immediately after the complete addition of 12 mmol Na_2HPO_4 (0.16 M) solution in the preparation of HAP coated GAC composite as given above. The pH of the mixture was maintained around 7. The washings were tested using UV–visible spectroscopy for the leaching of TE. The bi-coated nanocomposite obtained was characterized using FT-IR spectroscopy and scanning electron microscopy.

Filtering of an *Escherichia coli* bacterial suspension using column technique

The *E. coli* bacterial stock suspension was prepared by dissolving, isolated *E. coli* colonies from the previously prepared streaked plates, in 50 mL of double distilled autoclaved water. A sterile loop was used for transferring of bacteria. From the *E. coli* bacterial stock suspension, 100 times diluted bacterial suspension was prepared for the filtration. Lysogeny Broth (LB) Agar was used for the preparation of the culture media. The culture media was

Jayaweera *et al. Chemistry Central Journal* (2018) 12:18

Page 4 of 14

prepared by dissolving 25 g of LB and 20 g of Agar in 1 L of double distilled water.

Prior to filtering the *E. coli* bacterial suspension, GAC and the synthesized nanocomposites were autoclaved. Then 5 g of GAC, HAP/GAC and HAP/TE/GAC nanocomposites were packed into three separate columns with 12 mm diameter. The filter material was wetted with double distilled autoclaved water prior to filtering the *E. coli* bacterial suspension. A portion of 100 mL of the bacterial suspension was allowed to drain through the filter in the rate of 0.5 mL/min. The filtrate was collected in 10 mL fractions into autoclaved test tubes and kept in an ice bath to inhibit the bacterial growth. The *E. coli* bacterial content of these water samples was analyzed using the spread plate method, where 100 µL of each of the filtered fraction was spread in 15 mL of previously prepared LB Agar plate.

Heavy metal adsorption

Adsorption studies were carried out for Pb^{2+} ions in order to figure out the optimum adsorption conditions and adsorption capacity using adsorption isotherms. The Pb^{2+} standard stock solution (1000 ppm) was prepared using lead nitrate $Pb(NO_3)_2$. The other Pb^{2+} solutions, which were used for the studies, were prepared with necessary dilutions using Pb^{2+} standard stock solution. The adjustment of pH was done using dropwise addition of hydrochloric acid.

The effect of pH on the adsorption capabilities of neat GAC and the synthesized GAC nanocomposites was studied in the pH range of 4–7. The concentration of the Pb^{2+} ion solution (1000 ppm), amount of the adsorbent (1.0 g) and the volume (100.0 cm³) were kept constant for 180 min of contact time with random stirring. The experiment was performed under room temperature.

The effect of contact time on the adsorption capacities of GAC and the synthesized nanocomposites was investigated by using a known concentration of Pb^{2+} ion solution (1000 ppm, 100.0 cm³) in the time span of 15–180 min. The temperature was kept constant at room temperature with random stirring. The adsorbent was subjected to filtration from the solution and the filtrate was analyzed using atomic absorption spectroscopy for the residual Pb^{2+} ion concentration. The adsorption capacity was evaluated using the general equation given below.

$$Q_e = \frac{(C_o - C_e)V}{m} \quad (1)$$

where Q_e is the amount of Pb^{2+} adsorbed on the adsorbent (mg/g) C_o and C_e are the Pb^{2+} concentration in solution before and after the adsorption (mg/dm³) respectively, *m* is the amount of matter in the reaction mixture (g) and *V* is the volume of the medium (dm³).

Adsorption isotherms analysis of Pb^{2+} ions with GAC and the synthesized nanocomposites were carried out by keeping a constant amount of adsorbent (1.0 g) and volume (100.0 cm³) of different initial concentration of Pb^{2+} ion solution. The Pb^{2+} ion solutions with different initial concentrations (400, 500, 600, 700 ppm) were prepared by using the 1000 ppm standard stock solution. The pH of the solutions was maintained at pH 6 (experimentally determined optimum pH for the studies) and the solution mixture was equilibrated for 165 min (experimentally determined contact time for the analysis). The adsorbent was filtered and the amount of Pb^{2+} ions in the filtrate was determined by AAS after necessary dilutions.

The adsorption equilibrium data for Pb^{2+} ions on GAC and the synthesized nanocomposites were analyzed using the Freundlich and Langmuir isotherm models. The Freundlich isotherm is given by Eq. (2) where Q_e is the amount adsorbed per unit weight of the adsorbent (mg/g), C_e is the equilibrium metal ion concentration in the solution (mg/dm³) and K_f and *n* are Freundlich isotherm constants, related to the adsorption capacity and adsorption intensity respectively [40, 41].

$$\log Q_e = \log K_f + \frac{1}{n} \log C_e \quad (2)$$

The graph of $\log Q_e$ vs $\log C_e$ plotted to determine the Freundlich isotherm constants.

The Langmuir isotherm linearized form written as given in Eq. (3) where the constants q_m and *K*, are related to the adsorption capacity and the energy of adsorption, respectively. The graph of C_e/Q_e vs C_e was plotted to determine the Langmuir isotherm constants [42, 43].

$$\frac{C_e}{Q_e} = \frac{1}{q_m K} + \frac{C_e}{q_m} \quad (3)$$

Results and discussion

Characterization of HAP and HAP coated GAC

The formation of HAP coated GAC was confirmed by recording the FT-IR spectra and analyzing the characteristic peaks corresponding to the functional groups present in both HAP and GAC. Figure 1 shows the comparison of FT-IR spectra obtained for GAC, HAP and HAP coated GAC.

In the FT-IR spectrum of GAC (Fig. 1-GAC), the broad peak that appears at 3200–3600 cm⁻¹ region accounts for O–H stretching vibration in hydroxyl groups. The band at 1639 cm⁻¹ is ascribed to C=O stretching vibration in carboxylic groups. The peak in the region of 1565 cm⁻¹ is attributed to the C=C stretching mode in aromatic rings [44]. The sharp peak observed at 1384 cm⁻¹ accounts for C–O–H stretching in carboxylic groups. The peaks between 1249 and 1037 cm⁻¹ are assigned to C–O stretching vibration in alcohol and phenol groups. The
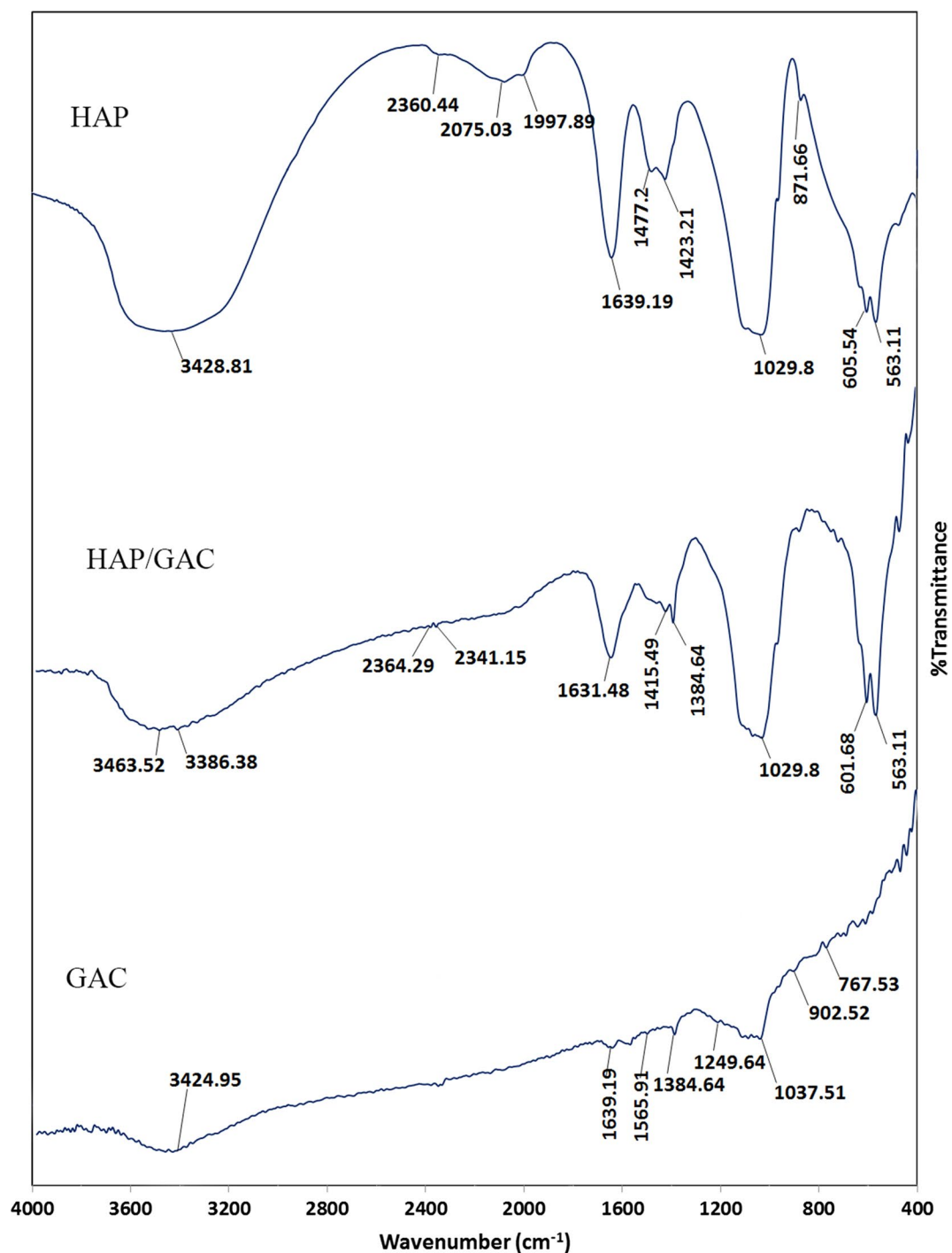
Jayaweera *et al. Chemistry Central Journal* (2018) 12:18

Page 5 of 14

Fig. 1 Comparison of FT-IR spectra of HAP, GAC and HAP/GAC

weaker bands between 902 and 767 cm^{-1} are ascribed to C–H bending in the aromatic rings [44].

The FT-IR spectrum of HAP (Fig. 1-HAP), the broad peak observed at 3700–3200 cm^{-1} is attributed to the stretching vibration mode of hydrogen bonded O–H

and the peak at 1639 cm^{-1} is due to adsorbed H_2O molecules. The peaks at 563, 960, 1029, 1083, 2360 cm^{-1} are assigned to PO_4^{3-} group stretching mode and the peaks at 605, 871 cm^{-1} accounts for the bending mode of PO_4^{3-} group [45, 46]. Thus, from analyzing the characteristic IR

Jayaweera *et al. Chemistry Central Journal* (2018) 12:18

Page 6 of 14

peaks in the FT-IR spectrum of HAP, it can be stated that the synthesized nanoflakes were HAP. The FT-IR spectrum of HAP coated GAC (Fig. 1-HAP/GAC) shows all prominent peaks at 563, 601, 1029 cm^{-1} corresponding to HAP nanoflakes. Thus, it can be stated that GAC has been coated with HAP to give HAP/GAC nanocomposites. In addition, the composite was further characterized using SEM and XRD.

The SEM micrographs obtained for HAP/GAC nanocomposite with different magnifications are given in Fig. 2. The size and the morphology of the synthesized HAP nanoflakes on GAC was determined using scanning electron microscopy. The HAP comprised of high percentage of flake shape morphology and they are connected to a continuous mesh with a width less than 100 nm and varied in length. The SEM image obtained for HAP/GAC displays almost a uniform coating of nano HAP over GAC. Nevertheless, the coating of HAP nanoflakes have not blocked the pores of the GAC as previously observed [22], which can be considered as an advantage since most of the adsorption of GAC occurs at the pore sites in the GAC [47]. This composite was subjected to the X-ray diffractometry for further confirmation of the coating of HAP on GAC and given in Fig. 3.

The peaks observed with noise at the 2Ө regions 26 and 42 can be assigned to GAC [48]. The peaks corresponding to neat HAP were not clear and this may be due to the low crystallinity of synthesized material. The observed XRD pattern for the HAP/GAC indicated that the HAP coated on the surface of GAC is not crystalline [26] but amorphous [22].

Characterization of turmeric extract, HAP bi-coated granular activated carbon

The HAP/GAC was further functionalized using the turmeric extract as given in the experimental section. The characterization of the curcuminoid pigments in the turmeric extract was carried out using FT-IR and UV–visible spectra. The comparison of FT-IR spectra for the original turmeric extract, HAP/TE/GAC and HAP/GAC are given in Fig. 4. The broad peak in the range of 3200–3600 cm^{-1} in neat turmeric extract can be attributed to the hydrogen bonded hydroxyl groups that are connected to the benzene rings in curcuminoids. The peak at 1627 cm^{-1} is due to the aryl substituted C=C bond. The peaks in the range of 2800–3000 cm^{-1} correspond to the C-H stretching of OCH$_3$ groups [49]. The stretching vibrations of C=O group result the peak at 1600 cm^{-1} where it generally appear at much higher range [50]. The IR bands arising from curcuminoid pigments are having similar positions except for the region of 2500–3000 cm^{-1} as shown in Fig. 4.

Curcumin gives rise to a FT-IR band in the region of 2980–2850 cm^{-1} and demethoxycurcumin exhibits a band in the region of 2950–2850 cm^{-1} while bisdemethoxycurcumin does not show any characteristic band due to the absence of C–H stretching regions corresponding to the OCH$_3$ groups [49]. Through the analysis of the FT-IR spectra in Fig. 4, it is clear that there are peaks in the region of 2850–2980 cm^{-1} in the turmeric extract justifying the presence of curcuminoids. The FT-IR spectrum for HAP/TE/GAC shows all peaks corresponding to the functional groups in the turmeric extract.

Figure 5 displays the physical appearance of the HAP/TE/GAC nanocomposite with the neat GAC and HAP/GAC. The neat GAC appears as black and this has become greyish with the coating of HAP. Successful coating of turmeric extract on HAP/GAC is clearly visible from the yellow colored HAP/TE/GAC composite.

Turmeric extract was further characterized by UV–visible spectroscopy and the spectrum obtained for the turmeric extract in ethanol is shown in Fig. 6.

Curcuminoids dissolved in ethanol exhibits characteristic UV-visible peaks at 429 nm, 424 nm and
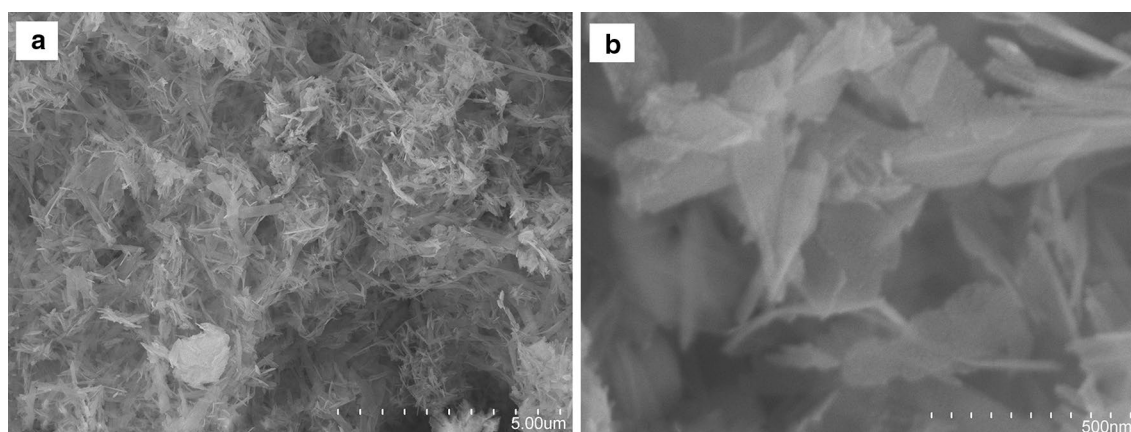
Fig. 2 SEM images of HAP/GAC nanocomposite with different magnifications **a** 5.00 μm, **b** 500 nm

Jayaweera *et al. Chemistry Central Journal* (2018) 12:18
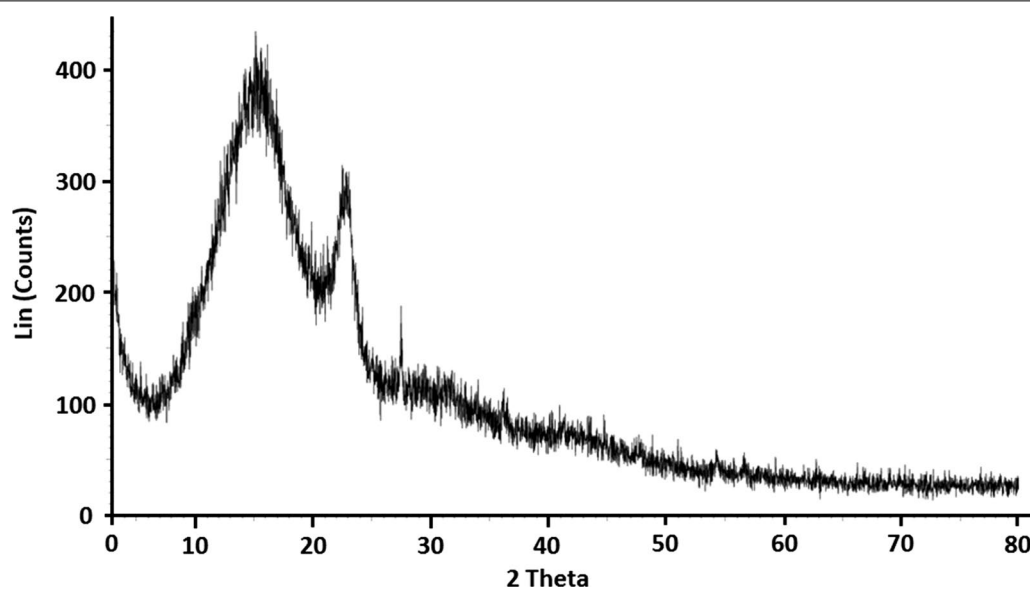
Page 7 of 14

Fig. 3 The XRD pattern of HAP/GAC

419 nm for curcumin, demethoxycurcumin and bisdemethoxycurcumin respectively [49]. As the sample contains all three pigments broader absorbance peak was observed between 418–432 nm with a maximum absorbance at 430 nm. Thus, it confirms the fact that turmeric extract used for the synthesis of nanocomposites contain curcuminoids.

The surface morphology of the HAP/TE/GAC was characterized using SEM (Fig. 7). Figure 7a and b represents only the HAP coated GAC and Fig. 7c and d represents turmeric extract coated HAP/GAC system (HAP/TE/GAC). Comparison of Fig. 7a–d indicates the presence of an additional solid material dispersed in between the HAP mesh. The deposition of turmeric extract had happened as flakes in between the mesh of nano HAP on the surface of the composite as shown in the diagram. The sizes of these flakes are almost in the micrometer range.

Filtering of an *Escherichia coli* bacterial suspension using column technique

The ability of removing bacteria by the composites was investigated using a known amount of *E. coli* bacterial suspension. This bacterial suspension was passed through columns packed with GAC, HAP/GAC and HAP/TE/GAC. The filtrate was collected as 10 mL aliquots as given in the methodology. Each fraction including original (initial) *E. coli* bacterial suspension was analyzed using impregnation method. The results obtained were the average number of colony forming units (CFUs) in 100 µL aliquot of the samples, by considering one bacterial cell as one CFU and the obtained results are summarized in Fig. 8.

$$\text{Ratio of CFUs} = \frac{\text{Number of CFUs in the fraction of filtrate}}{\text{Number of CFUs in the initial bacterial suspension}}$$

According to the data given in Fig. 8, the lowest bacterial removing ability was exhibited by neat GAC. The ability of biofilm formation on GAC was also observed from results achieved during this experiment [26, 32]. Thus, it can be stated that GAC alone is not a good filter material for the filtration of bacterial contaminated water. Results also indicated a slight reduction of the antibacterial activity when going from first 10 mL to tenth 10 mL, which can be endorsed to the reduction of the active sites of nanomaterials and the accessibility of the antibacterial compounds for the binding of bacteria due to the filtering of a large volume of the bacterial suspension. According to results, the removing capacities shown by the nanocomposites of HAP/GAC and HAP/TE/GAC are slightly similar to each other. However, in almost in all the aliquots tested there was a small reduction of CFU in the composite HAP/TE/GAC. Similar antibacterial activity of the two filter materials, HAP/GAC and HAP/TE/GAC, is due to the presence of antibacterial material, HAP nanoflakes in both composites. Small increment in the antibacterial activity of the composite HAP/TE/GAC can be ascribed to the presence of curcuminoids. However, the absence of a significant change observed with CFU could be attributed to the fact that the amount of curcumin present in the turmeric extract used for the
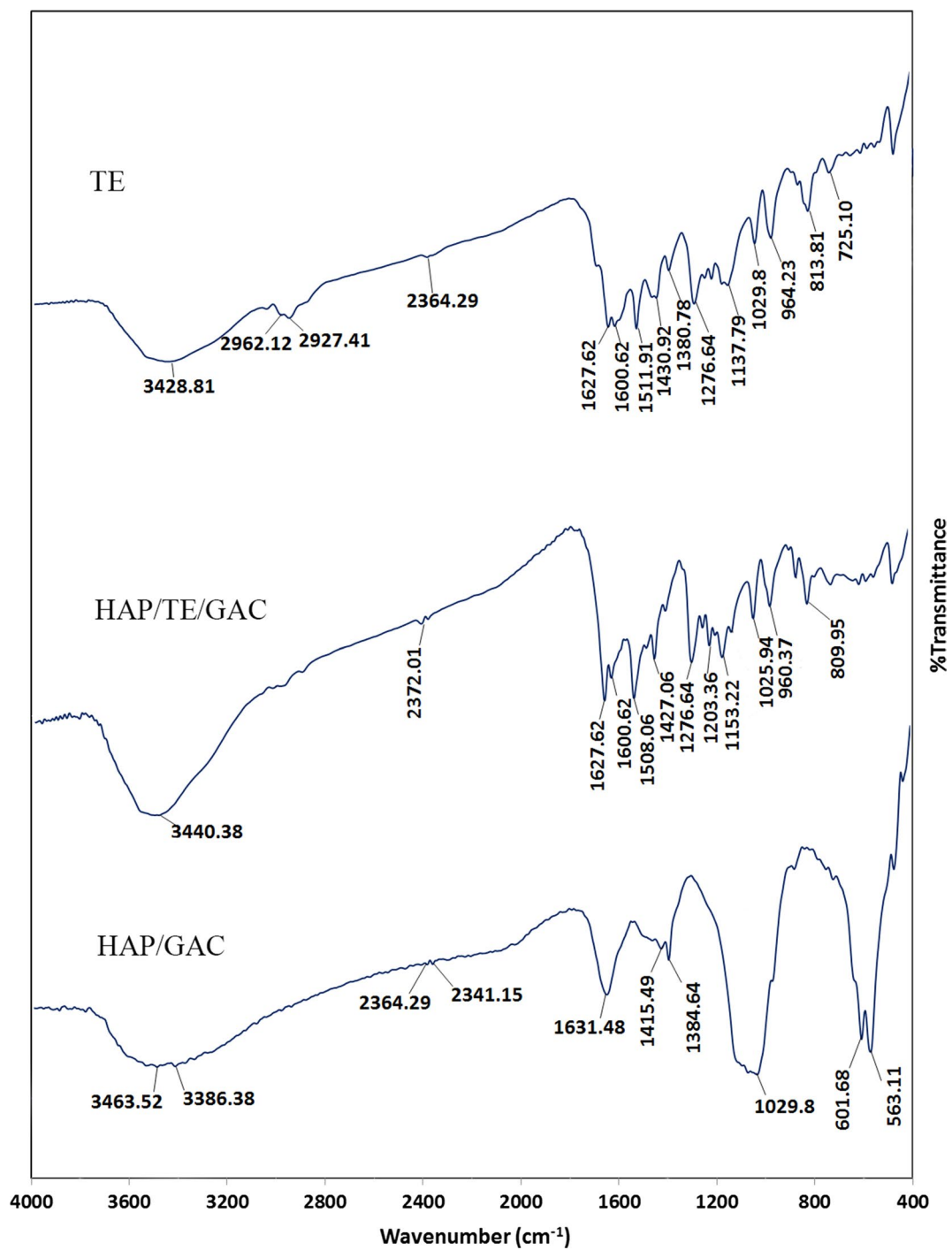
Jayaweera *et al. Chemistry Central Journal* (2018) 12:18

Page 8 of 14

Fig. 4 Comparison of FT-IR spectra of TE, HAP/GAC and HAP/TE/GAC

Jayaweera *et al. Chemistry Central Journal* (2018) 12:18

Page 9 of 14

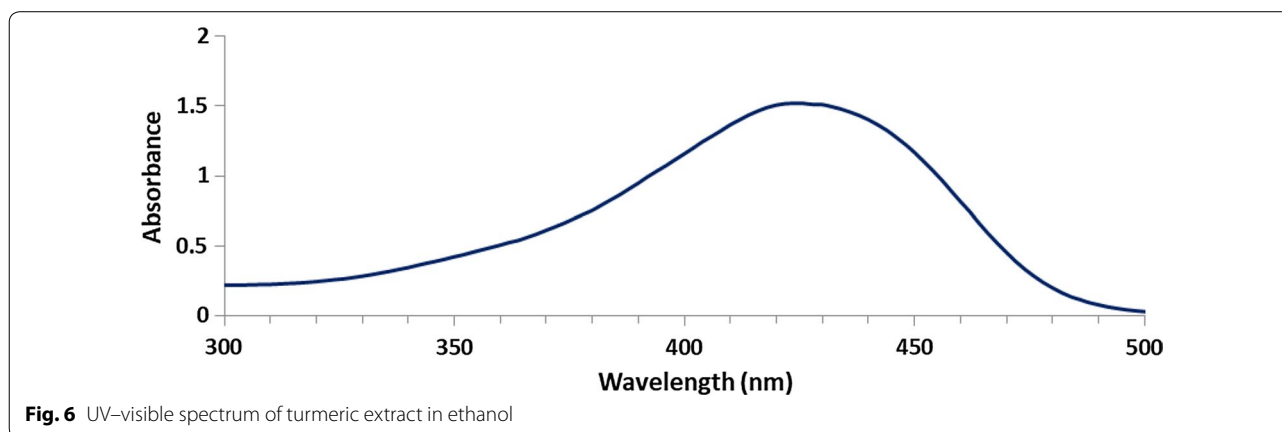**Fig. 5** Comparison of physical appearance of GAC, HAP/GAC and HAP/TE/GAC

Fig. 6 UV–visible spectrum of turmeric extract in ethanol

coating is less than the pure compound used in our previous study [26]. From this result, it is very clear that the synthesized nanocomposites can be categorized as bactericidal nanocomposites. The mechanism of action of curcumin in this system can be related to the inhibition of bacterial endotoxin induced cytokines secretion and related activation mechanisms, which directly suppresses bacterial cell growth as previously observed [39].

Adsorption studies of Pb^{2+} ions
Effect of pH
The results of the pH dependence on adsorption studies for GAC, HAP/GAC and HAP/TE/GAC are given in Fig. 9. In this study, pH lower than 4 was not considered as HAP is not stable. According to the graph, the adsorption capacities of three composites show similar trends with pH. However, the highest adsorption was observed with HAP/GAC as observed in earlier studies. Slightly lower adsorption capacity of the composite HAP/TE/GAC compared to neat GAC can be explained having a thick coating of TE on the surface of the composite. In addition, it is also clear from the SEM (Fig. 7) that TE extract had deposited on the surface of HAP coated GAC as flakes blocking some pore areas reducing the exposure of the surface area present in the HAP/GAC composite. The adsorption studies were carried out at pH 6, as previously reported [51].
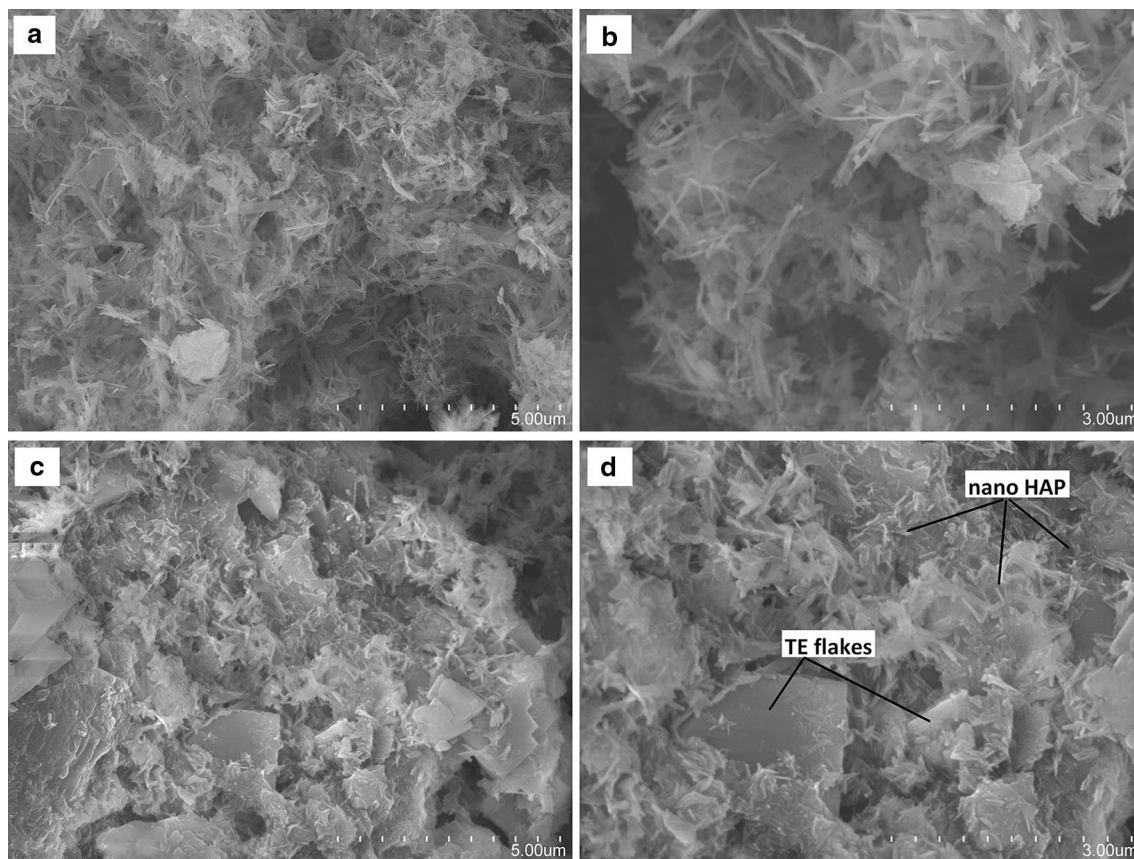
Jayaweera *et al. Chemistry Central Journal* (2018) 12:18

Page 10 of 14

Fig. 7 Comparison of SEM images of HAP/GAC **a** 5.00 µm, **b** 3.00 µm and HAP/TE/GAC **c** 5.00 µm, **d** 3.00 µm

Effect of contact time

The adsorption studies were carried out to determine the effect of contact time using a 1000 ppm Pb^{2+} ion solution as given in the methodology. The results are shown in Fig. 10 and according to that, the equilibrium concentration was reached for both GAC and HAP/GAC after about 135 min whereas HAP/TE/GAC takes 150 min to reach the equilibrium. Thus, after 150 min all the three composites have reached the equilibrium concentration. Therefore 165 min was taken as the contact time for further adsorption studies [22].

Adsorption isotherms for neat GAC, HAP/GAC and HAP/TE/GAC composites

The adsorption isotherm studies of Pb^{2+} ions on neat GAC, HAP/GAC and HAP/TE/GAC were carried out by keeping the amount of composite constant at 1.0 g and by varying the Pb^{2+} ion concentrations from 400, 500,

600 and 700 ppm. In order to identify the best-suited model for the adsorption process, adsorption isotherms were plotted using both Freundlich and Langmuir models and results obtained are given in Fig. 11. According to adsorption isotherms, the equilibrium adsorption data correlates well with Freundlich isotherm model, which describes multilayer adsorption on heterogeneous surfaces, and Langmuir isotherm model that illustrates monolayer adsorption in the given Pb^{2+} ion concentration range.

According to the R^2 values of the isotherm plots for GAC, the Langmuir isotherm and the Freundlich isotherm showed nearly the same correlation coefficient values greater than 0.98 at the given Pb^{2+} ion concentration. Thus, the adsorption process could be described well with both isotherm models as reported in previous related work [52]. The isotherm plots for HAP/GAC, Langmuir isotherm model (0.9989) and the Freundlich
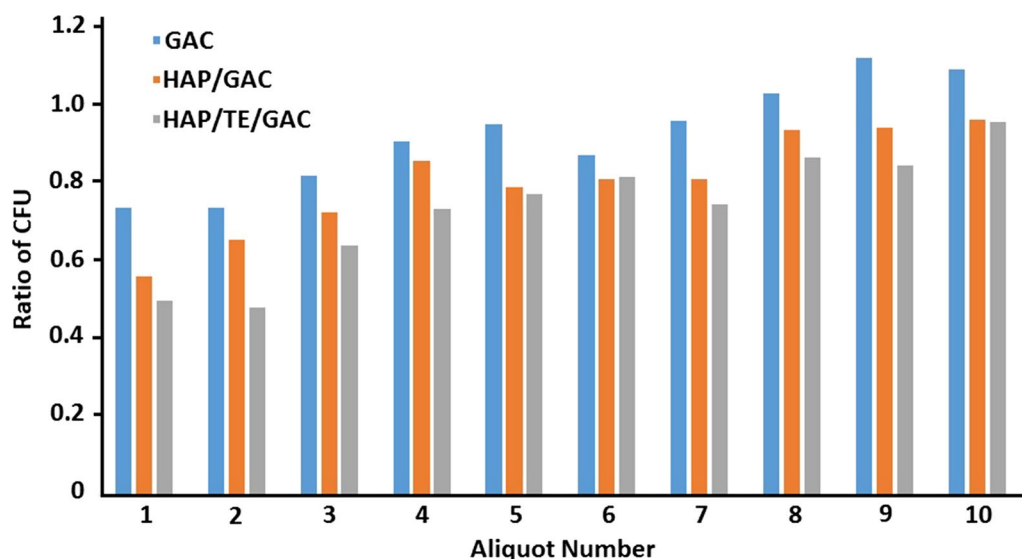
Jayaweera *et al. Chemistry Central Journal* (2018) 12:18

Page 11 of 14

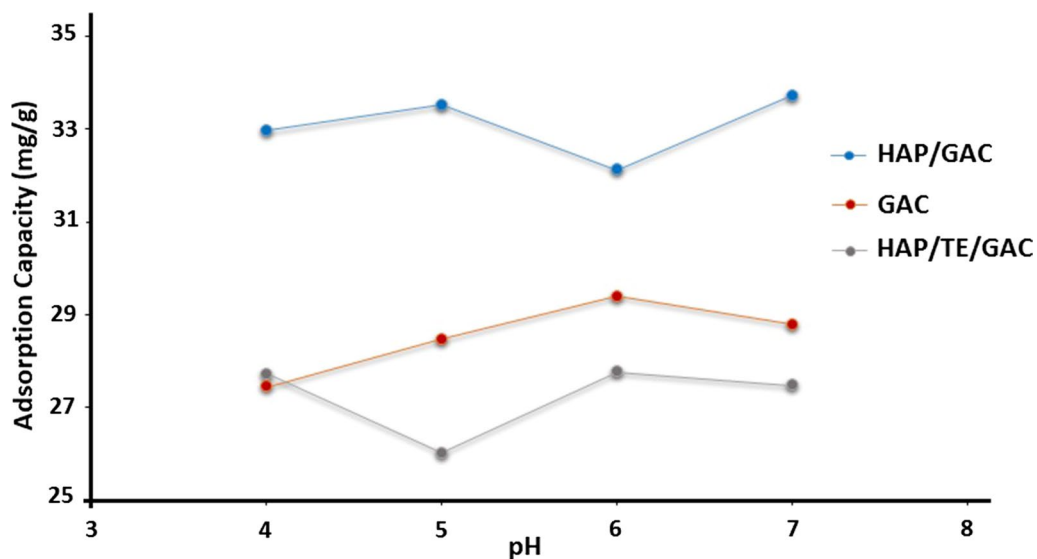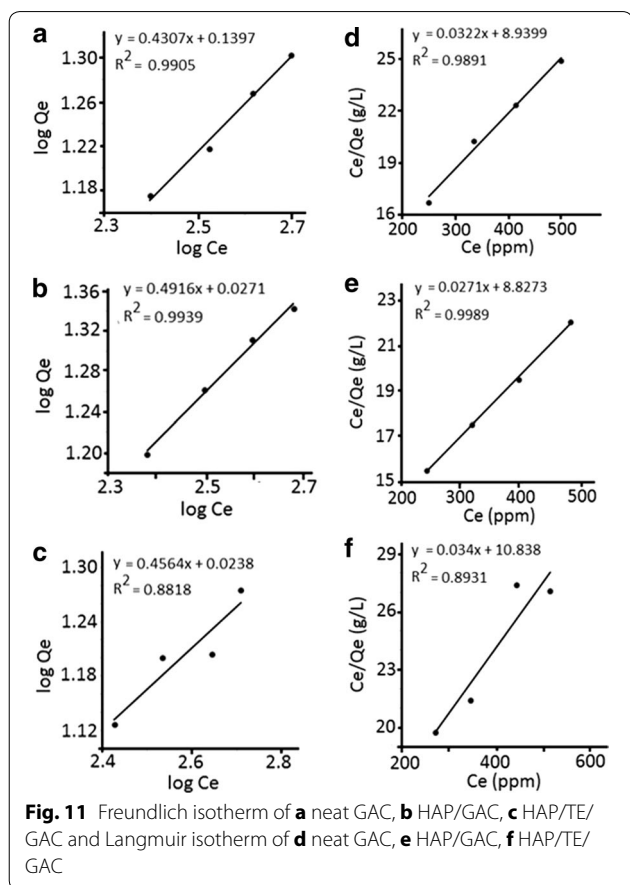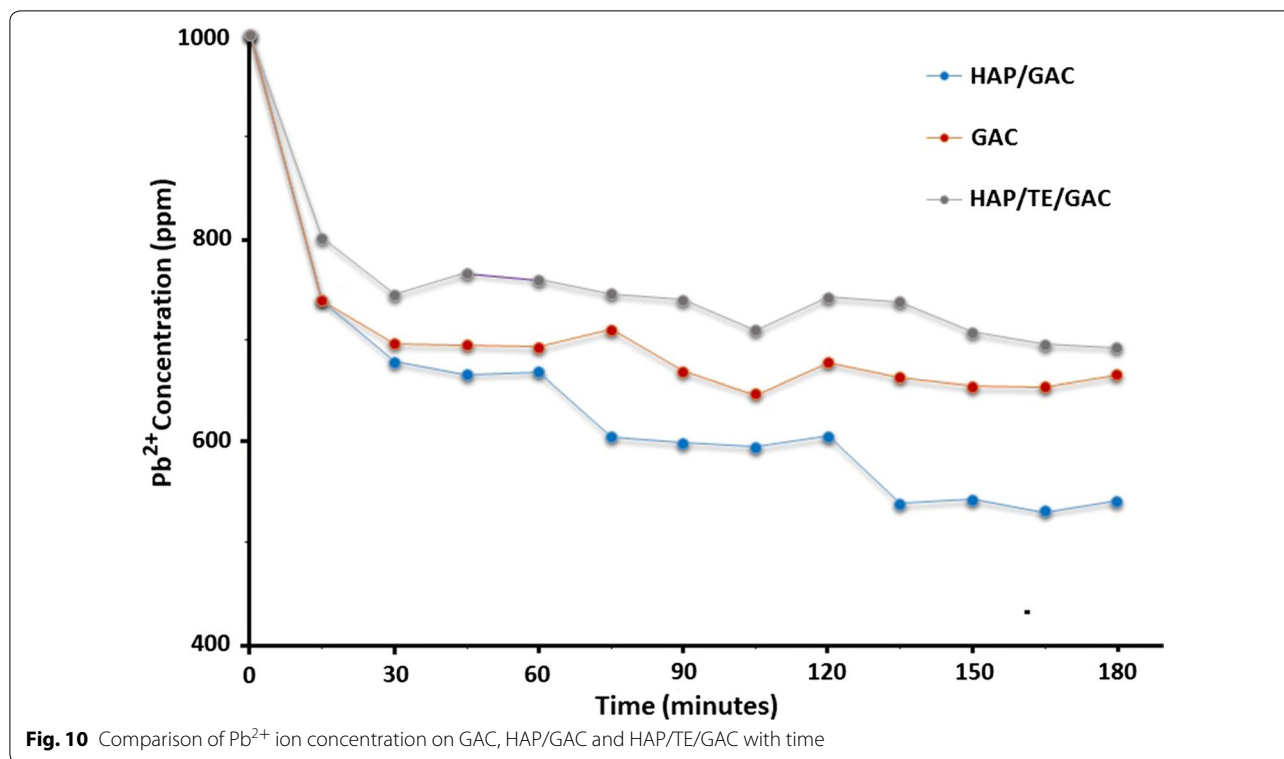**Fig. 8** Variation of different ratios of CFUs with sequential aliquots of filtrate

Fig. 9 Comparison of the adsorption capacity of Pb^{2+} on GAC, HAP/GAC and HAP/TE/GAC with pH

isotherm model (0.9939) gave almost the same correlation coefficient values in the given Pb^{2+} ion concentration. These values imply that the adsorption of Pb^{2+} on to HAP/GAC comply with both monolayer and multilayer adsorption on heterogeneous surface [22, 40, 52]. However, correlation coefficient values obtained for HAP/TE/

GAC composite showed slightly lower R^2 for both Langmuir and Freundlich models compared with neat GAC and HAP/GAC composite. This may be assumed to the presence of three types of adsorbate sites with different affinities towards Pb^{2+} ions.

Jayaweera *et al. Chemistry Central Journal* (2018) 12:18

Page 12 of 14

Fig. 10 Comparison of Pb^{2+} ion concentration on GAC, HAP/GAC and HAP/TE/GAC with time

Fig. 11 Freundlich isotherm of **a** neat GAC, **b** HAP/GAC, **c** HAP/TE/GAC and Langmuir isotherm of **d** neat GAC, **e** HAP/GAC, **f** HAP/TE/GAC

The adsorption constants were calculated using the slope and the intercept of the linear trendlines for the adsorption of Pb^{2+} by GAC, HAP/GAC and HAP/TE/GAC composites, are given in Table 1. The detailed adsorption data are included in the supporting materials. The adsorption capacity of HAP/TE/GAC was 29.4 mg of Pb^{2+} ions per 1 g of the composite. The results show that though HAP/GAC has the highest adsorption capacity among the composites, HAP/TE/GAC can also be used effectively in removing Pb^{2+} ions from aqueous solutions. In addition this composite is capable of removing bacteria and hence offsetting any reduced effect in metal ion removal and proving to be a multifunctional nanocomposite to purify water.

Conclusion

From the adsorption data it can be stated that 100 g of HAP/TE/GAC is capable of removing 2941.2 mg of Pb^{2+} ions from aqueous solution. It is also evident that the synthesized nanocomposite can be categorized as a bactericidal nanocomposite. Thus HAP/TE/GAC composite is capable of maintaining inherent properties of GAC while enhancing its capacity to remove heavy metals and bacterial contaminants. The biocompatible naturally occuring turmeric extract and HAP based activated carbon nanocomposite can be a strong contender to replace traditional silver and nanosilver based antibacterial filters

Jayaweera *et al. Chemistry Central Journal* (2018) 12:18

Page 13 of 14

Table 1 Langmuir and Freundlich adsorption isotherm constants for the adsorption of Pb^{2+} ions on to GAC, HAP/GAC and HAP/TE/GAC

Material	Langmuir adsorption isotherm constants			Freundlich adsorption isotherm constants		
	q_m (mg/g)	K (L/mg)	R^2	K_f	n	R^2
HAP/GAC	36.9 ($\pm$ 0.8)	3.1×10^{-3} ($\pm 1.1 \times 10^{-4}$)	0.9989	1.1 ($\pm$ 0.2)	2.0 ($\pm$ 0.1)	0.9939
GAC	31.1 ($\pm$ 2.3)	3.6×10^{-3} ($\pm 4.6 \times 10^{-4}$)	0.9891	1.4 ($\pm$ 0.2)	2.3 ($\pm$ 0.2)	0.9905
HAP/TE/GAC	29.4 ($\pm$ 7.2)	3.1×10^{-3} ($\pm 1.2 \times 10^{-3}$)	0.8931	1.1 ($\pm$ 0.7)	2.2 ($\pm$ 0.6)	0.8818

which are detrimental to the environment due to various reasons.

Additional file

Additional file 1. Additional tables.

Author details

[1] Department of Chemistry, University of Colombo, Colombo 00300, Sri Lanka. [2] Sri Lanka Institute of Nanotechnology (SLINTEC), Nanotechnology and Science Park, Mahenwatta, Pitipana, Homagama 10200, Sri Lanka.

Competing interests

The authors declare that they have no competing interests.

Availability of data and materials

Yes. All data provided in the manuscript. Additional file 1 is available.

Consent for publication

Yes (granted).

Ethics approval and consent to participate

Not applicable.

Publisher's Note

Springer Nature remains neutral with regard to jurisdictional claims in published maps and institutional affiliations.

References

1. Savage N, Diallo MS (2005) Nanomaterials and water purification: opportunities and challenges. J Nanoparticle Res 7(4–5):331–342
2. Amuda OS, Giwa AA, Bello IA (2007) Removal of heavy metal from industrial wastewater using modified activated coconut shell carbon. Biochem Eng J 36(2):174–181
3. World Health Organization (2011) Guidelines for drinking-water quality, 4th edn. World Health Organization, Geneva
4. Duruibe JO, Ogwuegbu MOC, Egwurugwu JN (2007) Heavy metal pollution and human biotoxic effects. Int J Phys Sci 2(5):112–118
5. Türkdoğan MK, Kilicel F, Kara K, Tuncer I, Uygan I (2003) Heavy metals in soil, vegetables and fruits in the endemic upper gastrointestinal cancer region of Turkey. Environ Toxicol Pharmacol 13(3):175–179
6. Jarup L (2003) Hazards of heavy metal contamination. Br Med Bull 68(1):167–182
7. Environmental Protection Agency (2011) Water treatment manual: disinfection. Environmental Protection Agency, Ireland, pp 22–97
8. Alvarez MT, Crespo C, Mattiasson B (2007) Precipitation of Zn(II), Cu(II) and Pb(II) at bench-scale using biogenic hydrogen sulfide from the utilization of volatile fatty acids. Chemosphere 66(9):1677–1683
9. Chen Q, Luo Z, Hills C, Xue G, Tyrer M (2009) Precipitation of heavy metals from wastewater using simulated flue gas: sequent additions of fly ash, lime and carbon dioxide. Water Res 43(10):2605–2614
10. Abo-Farha SA, Abdel-Aal AY, Ashour IA, Garamon SE (2009) Removal of some heavy metal cations by synthetic resin purolite C100. J Hazard Mater 169(1–3):190–194
11. Motsi T, Rowson NA, Simmons MJH (2009) Adsorption of heavy metals from acid mine drainage by natural zeolite. Int J Min Process 92(1–2):42–48
12. Kang KC, Kim SS, Choi JW, Kwon SH (2008) Sorption of Cu^{2+} and Cd^{2+} onto acid- and base-pretreated granular activated carbon and activated carbon fiber samples. J Ind Eng Chem 14(1):131–135
13. Kongsuwan A, Patnukao P, Pavasant P (2009) Binary component sorption of Cu(II) and Pb(II) with activated carbon from *Eucalyptus camaldulensis* Dehn bark. J Ind Eng Chem 15(4):465–470
14. Chen G (2004) Electrochemical technologies in wastewater treatment. Sep Purif Technol 38(1):11–41
15. Kabdaşlı I, Arslan T, Ölmez-Hancı T, Arslan-Alaton I, Tünay O (2009) Complexing agent and heavy metal removals from metal plating effluent by electrocoagulation with stainless steel electrodes. J Hazard Mater 165(1–3):838–845
16. Shahalam AM, Al-Harthy A, Al-Zawhry A (2002) Feed water pretreatment in RO systems: unit processes in the Middle East. Desalination 150(3):235–245
17. Ipek U (2005) Removal of Ni(II) and Zn(II) from an aqueous solution by reverse osmosis. Desalination 174(2):161–169
18. Zhong L-S, Hu J-S, Liang H-P, Cao A-M, Song W-G, Wan L-J (2006) Self-assembled 3D flowerlike iron oxide nanostructures and their application in water treatment. Adv Mater 18(18):2426–2431
19. Yantasee W, Warner CL, Sangvanich T, Addleman RS, Carter TG, Wiacek RJ et al (2007) Removal of heavy metals from aqueous systems with thiol functionalized superparamagnetic nanoparticles. Environ Sci Technol 41(14):5114–5119
20. Sheela T, Nayaka YA, Viswanatha R, Basavanna S, Venkatesha TG (2012) Kinetics and thermodynamics studies on the adsorption of Zn(II), Cd(II) and Hg(II) from aqueous solution using zinc oxide nanoparticles. Powder Technol 217:163–170
21. Mahdavi S, Jalali M, Afkhami A (2012) Removal of heavy metals from aqueous solutions using Fe$_3$O$_4$, ZnO, and CuO nanoparticles. J Nanoparticle Res 14(8):1–18
22. Fernando MS, de Silva RM, de Silva KMN (2015) Synthesis, characterization, and application of nano hydroxyapatite and nanocomposite of

Jayaweera *et al. Chemistry Central Journal* (2018) 12:18

Page 14 of 14

hydroxyapatite with granular activated carbon for the removal of Pb^{2+} from aqueous solutions. Appl Surf Sci 351:95–103

23. Wang H, Zhou A, Peng F, Yu H, Yang J (2007) Mechanism study on adsorption of acidified multiwalled carbon nanotubes to Pb(II). J Colloid Interface Sci 316(2):277–283

24. Kuo C-Y, Lin H-Y (2009) Adsorption of aqueous cadmium (II) onto modified multi-walled carbon nanotubes following microwave/chemical treatment. Desalination 249(2):792–796

25. Li Y, Liu F, Xia B, Du Q, Zhang P, Wang D et al (2010) Removal of copper from aqueous solution by carbon nanotube/calcium alginate composites. J Hazard Mater 177(1–3):876–880

26. Udayakantha KSM, de Silva RM, de Silva KMN, Hettiarachchi C (2015) Biocompatible nano hydroxyapatite–curcumin bi-coated antibacterial activated carbon for water purification. RSC Adv 5(79):64696–64703

27. Musee N, Thwala M, Nota N (2011) The antibacterial effects of engineered nanomaterials: implications for wastewater treatment plants. J Environ Monit 13(5):1164–1183

28. Wei C, Lin WY, Zainal Z, Williams NE, Zhu K, Kruzic AP et al (1994) Bactericidal activity of TiO_2 photocatalyst in aqueous media: toward a solar-assisted water disinfection system. Environ Sci Technol 28(5):934–938

29. Li Q, Mahendra S, Lyon DY, Brunet L, Liga MV, Li D et al (2008) Antimicrobial nanomaterials for water disinfection and microbial control: potential applications and implications. Water Res 42(18):4591–4602

30. Lyon DY, Fortner JD, Sayes CM, Colvin VL, Hughes JB (2005) Bacterial cell association and antimicrobial activity of a C_{60} water suspension. Environ Toxicol Chem 24(11):2757–2762

31. Udayakantha KSM, de Silva RM, de Silva KMN (2015) Nano-enriched granular activated carbon as a water filter matrix with heavy metal adsorption. In: Nano technology conference

32. Kamrin M, Hayden N, Christian B, Bennack D, D'Itri F (1990) A guide to home water treatment. Michigan State University Extension, East Lansing. Disponible de: http://www.gem.msu.edu/pubs/msue/wq21p1.html

33. Marsh H, Reinoso FR (2006) Activated carbon. Elsevier Science & Technology Books, London, pp 1–9

34. Pradeep T (2009) Noble metal nanoparticles for water purification: a critical review. Thin Solid Films 517(24):6441–6478

35. Lal J (2012) Turmeric, curcumin and our life: a review. Bull Env Pharmacol Life Sci 1(June):11–17

36. Benassi R, Ferrari E, Lazzari S, Spagnolo F, Saladini M (2008) Theoretical study on curcumin: a comparison of calculated spectroscopic properties with NMR, UV–Vis and IR experimental data. J Mol Struct 892(1–3):168–176

37. Stankovic I (2004) Curcumin: chemical and technical assessment (CTA). 61st JECFA© FAO

38. Cui J, Yu B, Zhao Y, Zhu W, Li H, Lou H et al (2009) Enhancement of oral absorption of curcumin by self-microemulsifying drug delivery systems. Int J Pharm 371(1–2):148–155

39. Liang G, Yang S, Jiang L, Zhao Y, Shao L, Xiao J et al (2008) Synthesis and anti-bacterial properties of mono-carbonyl analogues of curcumin. Chem Pharm Bull (Tokyo) 56(2):162–167

40. Adamson AW (1979) A textbook of physical chemistry, 2nd edn. Academic Press, New York

41. Castellan GW (1983) Physical chemistry, 3rd edn. Addison-Wesley, Boston

42. Duff DG, Ross SMC, Vaughan DH (1988) Adsorption from solution: an experiment to illustrate the Langmuir adsorption isotherm. J Chem Educ 65(9):815

43. Dunicz BL (1961) Surface area of activated charcoal by Langmuir adsorption isotherm. J Chem Educ 38(7):357

44. Allwar A (2012) Characteristics of pore structures and surface chemistry of activated carbons by physisorption, Ftir And Boehm methods. IOSR J Appl Chem 2(1):09–15

45. Han J-K, Song H-Y, Saito F, Lee B-T (2006) Synthesis of high purity nano-sized hydroxyapatite powder by microwave-hydrothermal method. Mater Chem Phys 99(2–3):235–239

46. Chen L, Mccrate JM, Lee JC-M, Li H (2011) The role of surface charge on the uptake and biocompatibility of hydroxyapatite nanoparticles with osteoblast cells. Nanotechnology 22(10):105708

47. Kannan N, Veemaraj T (2010) Detoxification of toxic metal ions by sorption onto activated carbon from *Hevea brasiliensis* bark—a comparative study. Glob NEST 12(2):197–205

48. Mopoung S (2008) Surface image of charcoal and activated charcoal from banana peel. J Microsc Soc Thai 22:15–19

49. Péret-Almeida L, Cherubino APF, Alves RJ, Dufossé L, Glória MBA (2005) Separation and determination of the physico-chemical characteristics of curcumin, demethoxycurcumin and bisdemethoxycurcumin. Food Res Int 38(8–9):1039–1044

50. Paradkar A, Ambike AA, Jadhav BK, Mahadik KR (2004) Characterization of curcumin—PVP solid dispersion obtained by spray drying. Int J Pharm 271(1–2):281–286

51. Ramesh ST, Rameshbabu N, Gandhimathi R, Srikanth Kumar M, Nidheesh PV (2013) Adsorptive removal of Pb(II) from aqueous solution using nano-sized hydroxyapatite. Appl Water Sci 3(1):105–113

52. Okeola FO, Odebunmi EO (2010) Comparison of Freundlich and Langmuir isotherms for adsorption of methylene blue by agrowaste derived activated carbon. Adv Environ Biol 4(3):329–335